https://doi.org/10.5194/acp-2022-284
Preprint. Discussion started: 1 June 2022

Atmospheric Chemistry and Physics Discussions

Evidence for mass independent fractionation of even mercury isotopes in the troposphere

Shuyuan Huang[1,2], Yunlong Huo[1], Heng Sun[1], Supeng Lv[1], Yuhan Zhao[1,2], Kunning Lin[1], Yaojin Chen[2], Yuanbiao Zhang[1*]

[1]*Third Institute of Oceanography, Ministry of Natural Resources, Xiamen, Fujian 361005, China*

[2]*State Key Laboratory of Marine Environmental Science, Xiamen University, Xiamen, Fujian 361102, China*

[*]*Corresponding author: zhangyuanbiao@tio.org.cn*

Abstract: Mass independent fractionation (MIF) of even mercury (Hg) isotopes has long been observed in atmospheric related samples and is confirmed to be generated in the atmosphere, but its exact mechanism is covered up by the Hg sources and atmospheric transformations and stays unclear. Here, we present the first Hg isotope compositions of particulate bound mercury (PBM) in the Northwest Pacific and observe highly positive Δ^{200}Hg values (up to 0.42‰). The MIF signatures are mainly controlled by photoreduction, gaseous elemental mercury (GEM) oxidation, and even-MIF dominated oxidation processes. Mercury in a small part of samples influenced by anthropogenic emissions is recognized by Hg concentrations and Δ^{199}Hg signatures. The correlation between Δ^{200}Hg and light conditions confirms that even-MIF is linked to photochemical reactions. The correlation between Δ^{200}Hg and altitudes

https://doi.org/10.5194/acp-2022-284
Preprint. Discussion started: 1 June 2022


Atmospheric Chemistry and Physics Discussions

suggests that a max even-MIF signatures existed in the troposphere. We use $\Delta^{199}Hg/\Delta^{200}Hg$ ratios and ternary isotopic mixing model to estimate the contributions of photoreduction, GEM oxidation and even-MIF dominated oxidation. Our results demonstrate that atmospheric transformations are far more important than Hg sources in shifting Hg isotope compositions of PBM samples, especially in the marine boundary layer of the open ocean, which is characterized by less anthropogenic influences and has implications for our understanding of the mechanism of even-MIF and subsequently Hg behaviors in the atmosphere.

https://doi.org/10.5194/acp-2022-284
Preprint. Discussion started: 1 June 2022


Atmospheric Chemistry and Physics Discussions

1. Introduction

Mercury (Hg) mainly exists in three forms in the atmosphere: gaseous elemental mercury (GEM), gaseous oxidized mercury (GOM), and particulate bound mercury (PBM). GOM and PBM both exhibit a short residence time in the atmosphere and are readily deposited near Hg sources. In contrast, GEM is subject to long range transport and can be deposited significant distances from emission sources, including in relatively remote regions of the planet [1]. Atmospheric Hg continuously undergoes complicated physical and chemical transformations, including photoreactions, dark abiotic redox reaction, adsorption, and desorption, before being incorporated into the underlying surface [2]. Extensive efforts have been made to measure and model Hg in the atmosphere [3]. Recent advances in Hg stable isotopes have greatly improved our understanding of Hg cycling in the environment, including within the atmosphere [4-6].

Mercury has seven stable isotopes (^{196}Hg, ^{198}Hg, ^{199}Hg, ^{200}Hg, ^{201}Hg, ^{202}Hg, and ^{204}Hg). Mass dependent fractionation (MDF) of Hg isotopes is widely observed in natural environments, whereas significant mass independent fractionation of odd mass Hg isotopes (odd-MIF) is mainly induced by photochemical reactions [7]. Significant MIF of even mass Hg isotopes (even-MIF) has been measured in atmospheric samples or samples that relates to atmospheric Hg source [8-14]. However, the exact mechanism triggering even-MIF is unclear [15]. It is generally speculated that specific

https://doi.org/10.5194/acp-2022-284
Preprint. Discussion started: 1 June 2022


Atmospheric Chemistry and Physics Discussions

oxidation reactions transforming Hg(0) to Hg(II) induced even-MIF. Fu et al. attributed even-MIF to surface-mediated Hg photoreduction involving halogens that can as of yet not explain [16]. Nonetheless, even-MIF signatures have become a useful tracer to constrain atmospheric Hg deposition pathways, reservoir size, and atmospheric conditions. Both MDF and MIF provide useful information to trace Hg sources and identify Hg transformation processes [13,16-18].

Isotopic compositions of PBM in urban and remote areas reflect differing controls including anthropogenic emissions and atmospheric transformations [19-23]. A recent study proposed that atmospheric transformations could induce more positive odd-MIF values in PBM than that from anthropogenic Hg sources [24]. Of marine boundary layer (MBL), most PBM data have been collected from ground platforms [2] and show that PBM plays an important role in the geochemical cycling of Hg. The MBL is the largest transport layer and reaction vessel of atmospheric Hg due to its relatively high humidity, sufficient sunlight, and abundant atmospheric oxidants [25,26]. To date, several studies have been conducted in the MBL over the open ocean and suggested that continental anthropogenic emissions have little contribution to Hg in the open seas MBL and GEM oxidation and photoreduction greatly shift isotopic compositions of Hg species (i.e., GEM, PBM) in the MBL [17,27]. Hence, the Hg isotope signatures in the MBL is of great significance to understand the

https://doi.org/10.5194/acp-2022-284
Preprint. Discussion started: 1 June 2022


Atmospheric Chemistry and Physics Discussions

transformation of atmospheric Hg. However, the relative contributions of GEM oxidation, photoreduction, and other atmospheric Hg transformation processes is rarely quantified and reported.

This study investigated the distribution and source of PBM in the MBL over the Northwest Pacific Ocean and the associated controlling factors on even-MIF. PBM samples were collected during three cruises and subsequently analyzed for selected Hg isotopes. The isotopic compositions of the PBM were then combined with the Hybrid Single-Particle Lagrangian Integrated Trajectory (HYSPLIT) model [28,29] to identify the sources of PBM. Atmospheric transformations were identified by odd-MIF and even-MIF. We proposed two ways to quantify contributions from photoreduction, GEM oxidation, and even-MIF dominated photochemical reactions in troposphere using Hg isotopic compositions.

2. Methods

2.1 Study sections. Three Cruises were conducted in the Northwest Pacific during the periods from August to November 2019 (denoted as Cruise A), May to June 2018 (denoted as Cruise B), and August to September 2019 (denoted as Cruise C) (**Fig. 1**). Cruise A circumnavigated the southern portion of the Northwest Pacific (7.00–24.74°N), whereas Cruise B primarily navigated the western North Pacific around 30°N (21.00–37.02°N). Cruise C was extended from the northwest marginal sea of the

https://doi.org/10.5194/acp-2022-284
Preprint. Discussion started: 1 June 2022


Atmospheric Chemistry and Physics Discussions

North Pacific to the Bering Strait (34.52–73.34°N). Based on atmospheric circulation and the results of 120 h back-trajectory analysis of air masses from the HYSPLIT model, the northeast trade wind prevails at 0°N–30°N and the westerly wind prevails at 30°N–60°N in the North Pacific. Polar easterly winds prevail at high latitudes. The area of the South China Sea and Western Pacific sampled during Cruise A is affected by the southwest monsoon, while Northeast Asia, sampled during Cruise B, is controlled by the northwest monsoon.

2.2 Sample collection. Two ARA N-FRM samplers (ARA Instruments, USA) were deployed on the compass deck of the research vessel at a height of approximately 15 m above mean sea level (AMSL) and at about 10 m upstream of the exhaust outlet. To reduce the potential for contamination from the ship's exhaust plume, sampling was stopped during station work and when bad weather was encountered. Quartz fiber membranes (Grade QMA, 47 mm, Whatman) were used for the collection of PBM as outlined in a previous study [21]. The sampling time of each sample lasted for 48–72 h at a flow rate of about 20 L/min.

2.3 Sample preconcentration. PBM on the membrane was released via a dual-stage tube furnace combustion protocol [21,30]. A $KMnO_4$ trapping solution (0.1% $KMnO_4$ (*m/v*) + 10% H_2SO_4 (*v/v*)) was utilized to capture

https://doi.org/10.5194/acp-2022-284
Preprint. Discussion started: 1 June 2022


Atmospheric Chemistry and Physics Discussions

the released Hg [21], after which it was preserved in the dark at 4°C until analyzed for Hg concentration and relative isotopic abundances. Mercury concentrations in the trapping solutions were measured by cold vapor atomic fluorescence spectrometry (CVAFS, MERX, Brooks Rand Instruments, USA) following US EPA Method 1631. PBM levels were so low that Hg concentrations in the trapping solutions were lower than 1.0 ng/L. Hg standard solutions (NIST 3133) were therefore added to ensure sufficient Hg mass (approximately 5 ng) for isotope analysis following our previous study (**Note S1**) [31].

2.4 Hg stable isotope analyses. Mercury isotopic compositions of the solutions were determined with a Nu Plasma Multi-Collector Inductively Coupled Plasma Mass Spectrometer (MC-ICPMS) housed at the State Key Laboratory of Marine Environmental Science at Xiamen University. A modified cold-vapor generator and an Aridus III desolvating nebulizer system (CETAC Technologies, USA) were used for Hg and thallium (Tl) introduction, respectively, following previously published methods [32]. The Hg isotopic compositions are reported in δ (‰) and Δ (‰) notation, which represents the MDF and MIF of the Hg isotopes, respectively [33], such that:

$$\delta^{xxx}Hg_{sample} = (({}^{xxx}Hg_{sample}/{}^{198}Hg_{sample}) / ({}^{xxx}Hg_{NIST3133}/{}^{198}Hg_{NIST3133}) - 1) \times 1000 \quad (5)$$

$$\Delta^{xxx}Hg = \delta^{xxx}Hg - \beta \times \delta^{202}Hg \quad (6)$$

https://doi.org/10.5194/acp-2022-284
Preprint. Discussion started: 1 June 2022


Atmospheric Chemistry and Physics Discussions

where xxx refers to the mass of each Hg isotope with atomic mass units (amu) of 199, 200, 201, and 202. The fractionation factor β is 0.2520, 0.5024, and 0.7520 for ^{199}Hg, ^{200}Hg, and ^{201}Hg, respectively.

The repeated measurements of NIST 8610 gave long-term average δ^{202}Hg, Δ^{199}Hg, and Δ^{200}Hg values of −0.52±0.12‰ (2SD, n=5), −0.02±0.04‰ (2SD, n=5), and 0.00±0.02‰ (2SD, n=5), respectively. These values are in accordance with previous studies [12,34,35]. Since the samples were measured only once, the 2SD of the isotopic compositions for each sample were selected as the 2SD of NIST 8610 (**Table S1**). The isotopic compositions of PBM and the corresponding uncertainties (see **Table S2**) were calculated by the method we previously developed [31]. Additional details pertaining to the approach are provided in the **Note S2**.

2.5 Quality assurance and quality control. Any unused pre-cleaned quartz filters were placed in the closed sampling systems for 2 d to obtain field blanks of PBM. In the process of sample preconcentration, unused pre-cleaned quartz filters were periodically combusted with the samples to obtain method blanks. For Hg isotopic analyses, the sample introduction system was rinsed between samples with 3% HNO_3 solution until the signal intensity dropped to background levels to avoid memory effects. Generally, the blanks accounted for <3% in all the trapping solutions. The dual-stage tube furnace combustion protocol was tested by adding NIST 3133 to

https://doi.org/10.5194/acp-2022-284
Preprint. Discussion started: 1 June 2022


Atmospheric Chemistry and Physics Discussions

unused pre-cleaned quartz filters. The recovery was 101±8% (n=6, 1SD).

Standard solutions (NIST 8610) were used as a substitute for samples and mixed with NIST 3133 in different proportions (33.3%, 50%, and 66.7%) to evaluate the isotopic compositions of PBM. The calculated isotopic compositions of NIST 8610 were −0.57±0.10‰ (1SD, n=8), −0.07±0.09‰ (1SD, n=8), and 0.01±0.04‰ (1SD, n=8) for δ^{202}Hg, Δ^{199}Hg, and Δ^{200}Hg, respectively (**Fig. S1**).

2.6 Backward trajectories of air masses and identification of potential source regions. Air mass transport to the sampling area was assessed using the NOAA Air Resources Laboratory GDAS 1° data archive and the HYSPLIT model. Trajectory frequencies were analyzed to identify the potential source as well as represent air mass transport. The trajectory frequency started a trajectory from a single location and height every 6 h and then summed the frequency that the trajectory passed over a grid cell. This data was then normalized by the total number of trajectories (**Fig. S2**). The parameter settings are shown in **Table S3**.

Locations of each sampling site are reported as the mean longitude and latitude of the starting and ending points of sampling. The start time used to run the model was chosen as the end date of sampling for each sample (**Table S2**). The backward trajectories were calculated at a height of 500 m AMSL and are representative of the approximate height of the

https://doi.org/10.5194/acp-2022-284
Preprint. Discussion started: 1 June 2022


Atmospheric Chemistry and Physics Discussions

MBL where atmospheric pollutants are well mixed.

2.7 Analyses of height of backward trajectories of air mass. 315 h backward trajectories of air mass arrived at 15 m height AMSL at each sampling site were calculated at 1 h intervals using HYSPLIT model. Three backward trajectories were output for each sampling site at starting point, intermediate point, and end point. A total of 948 height values were obtained for each sample. The frequency of trajectory points with height higher than 500 m, 1500 m, and 3000 m AMSL (f_{500}, f_{1500}, and f_{3000}) were calculated, respectively (**Table S4**). Furthermore, limit condition that trajectory points fall in day light (f_{500_light}, f_{1500_light}, and f_{3000_light}) was added to represent air mass originated from upper atmosphere and suffered from sunlight.

2.8 Estimation of the max Δ^{200}Hg values produced in the troposphere. For convenience, only three heights ($F_{\text{position}} < 1/18$, $1/18 < F_{\text{position}} < 1/6$, $F_{\text{position}} > 1/6$) were chose to calculate the max Δ^{200}Hg value based on the following equations:

$$f_a \times \Delta_a^{200}Hg_i + f_b \times \Delta_b^{200}Hg_i + f_c \times \Delta_c^{200}Hg_i = \Delta_{sam\_iv}^{200}Hg \quad (7)$$

$$f_a + f_b + f_c = 1 \quad (8)$$

where f_a, f_b, and f_c represent frequencies of trajectory points at a height of $F_{\text{position}} < 1/18$, $1/18 < F_{\text{position}} < 1/6$, and $F_{\text{position}} > 1/6$, respectively.

https://doi.org/10.5194/acp-2022-284
Preprint. Discussion started: 1 June 2022


Atmospheric Chemistry and Physics Discussions

$\Delta_a^{200}Hg_i$, $\Delta_b^{200}Hg_i$, $\Delta_c^{200}Hg_i$ represent Δ^{200}Hg values at the three heights and modeled by Monte Carlo simulation approach through the pseudorandam number generation (i=1:10000). $\Delta_{sam\_iv}^{200}Hg$ represent Δ^{200}Hg values of PBM samples of type v.

3. Results

3.1 PBM concentrations. PBM concentrations exhibited mean values of 16.1±9.2 pg/m^3 (n=33, 2SD) and 16.0±10.5 pg/m^3 (n=7, 2SD) during Cruises A and B, respectively (**Fig. 2a**). Concentrations were lower than continental boundary layer PBM in most areas, especially in East Asia, but higher than those in the MBL of the Pacific ocean (typically <10 pg/m^3) [2]. Long-term observations have shown that PBM concentrations are usually lower than 30 pg/m^3 in the free troposphere [36], and thus, similar to that found herein for the MBL.

Highly variable PBM concentrations (11.5–63.4 pg/m^3) were found in samples from Cruise C; the mean concentration was 31.8±32.8 pg/m^3 (n=12, 2SD). The lowest concentration was observed at station 41, which was in the Sea of Japan, while the highest concentration was observed at station 47, which was in the Bering Sea. Compared to Cruises A and B, Cruise C was closer to the coast. The elevated PBM concentrations in Cruise C may thus be due to anthropogenic influences.

https://doi.org/10.5194/acp-2022-284
Preprint. Discussion started: 1 June 2022


Atmospheric Chemistry and Physics Discussions

3.2 PBM isotope compositions. The isotope compositions of PBM collected from the MBL exhibited negative δ^{202}Hg (−0.98±1.46‰, n=52, 2SD) and variable Δ^{199}Hg values (−0.08±0.56‰, n=52, 2SD). The isotopic signatures overlapped with previously reported PBM isotope data. As shown in **Fig. 3**, the PBM collected from urban regions exhibited large variations in Δ^{199}Hg values (−0.02±0.61‰, n=205, 2SD) [19-23,37,38]. More positive Δ^{199}Hg values (0.40±0.71‰, n=128, 2SD) have been observed for PBM collected from areas of high altitude (from 50 m to 3816 m) [23,24]. The PBM collected from polar regions displayed positive δ^{202}Hg and negative Δ^{199}Hg values [11,13]. In contrast, the isotopic compositions of PBM collected from specific emission sources, such as vehicles, industry, waste, flue gas, and volcanos, have been characterized by negative δ^{202}Hg and near-zero Δ^{199}Hg [5,39,40]. In addition, significant positive Δ^{200}Hg values (0.14±0.30‰, n=52, 2SD) were observed in the current study (**Fig. 2d**).

Different isotopic signatures were found among different PBM samples within the same cruise and between different cruises (**Fig. 2 & Fig. S3**). Lower δ^{202}Hg values were observed near Micronesia and the Bering Sea during Cruises A and C, while higher δ^{202}Hg values were found during Cruise B (**Fig. 2b**). The spatial distribution of Δ^{199}Hg of PBM was more complicated (**Fig. 2c**). For Cruises A and B, positive Δ^{199}Hg values were mainly distributed in areas of open ocean in the Northwest Pacific, while negative Δ^{199}Hg values were dispersed. Positive and negative Δ^{199}Hg

https://doi.org/10.5194/acp-2022-284
Preprint. Discussion started: 1 June 2022


Atmospheric Chemistry and Physics Discussions

values were observed during Cruise C in the marginal sea of Northeast Asia and the Bering Sea, respectively.

4. Discussion

According to the Δ^{199}Hg values, PBM samples could be divided into two groups (**Fig. S4**): 1) samples characterized by positive Δ^{199}Hg values, which were related to the air mass from areas of open ocean (e.g., the Northwest Pacific and the marginal sea in Northeast Asia), and 2) samples possessing negative Δ^{199}Hg values related to the air mass from the South China Sea, Micronesia, Hawaii, Japan, Russia, and Bering Sea. Air mass source analysis was predicted by HYSPLIT model (see Methods).

Long-range transport from anthropogenic emissions in mid-latitude regions and GEM oxidation are two possible sources for the negative Δ^{199}Hg values of PBM [13]. The Δ^{199}Hg values are plotted against Hg concentrations in the PBM in **Fig. 4a**. Positive correlation are observed in PBM samples with negative Δ^{199}Hg values (**Fig. 4b**). The samples collected during Cruises B and C possess a stronger correlation (r^2=0.61, $p<0.05$) than the samples collected during Cruise A (r^2=0.04, $p>0.1$). The higher Hg concentrations in PBM are most likely caused by the long-range transport from anthropogenic emissions, which produced the slightly negative Δ^{199}Hg values. However, the significantly negative Δ^{199}Hg values associated with lower Hg concentrations in the PBM presumably result from the *in situ* GEM oxidation. A few data points with slightly negative

https://doi.org/10.5194/acp-2022-284
Preprint. Discussion started: 1 June 2022


Atmospheric Chemistry and Physics Discussions

278 Δ^{199}Hg deviate positively from the regression lines in **Fig. 4b**. These
279 samples was likely influenced by the photoreduction of Hg(II), which
280 induced positive Δ^{199}Hg values in residual Hg(II). Noted that the
281 background PBM pool is characterized by significant positive Δ^{199}Hg
282 values, which is also associated with photoreduction [24]. Hence, samples
283 related to the open ocean with highly positive Δ^{199}Hg values are mainly
284 controlled by photoreduction.

285 A large variation range of δ^{202}Hg values are observed for PBM
286 samples with both positive and negative Δ^{199}Hg values (**Fig. 4c**).
287 According to previous study, strong photoreduction of Hg(II) induced
288 positive shift of δ^{202}Hg values in reactants (e.g., PBM) [27,41]. Although
289 inverse kinetic isotope effect was observed in Hg(0) oxidation by Cl and
290 Br atoms [42], the subsequent adsorption of Hg(II) on particulate surfaces
291 would lead to negatively shift of δ^{202}Hg values in PBM. Furthermore, GEM
292 originated from dissolved gaseous mercury displayed more negative
293 δ^{202}Hg (−2.98 to −0.99‰) [14] than that in the upper atmosphere (−0.02 to
294 1.64‰) [43,44], indicating that it is difficult to identify Hg source with δ^{202}Hg
295 values. In addition to photochemical and redox reactions, gas-particle
296 partitioning, dissolution, and evaporation would also affect δ^{202}Hg values
297 in PBM. Moreover, no correlation was found between δ^{202}Hg values and
298 Hg concentrations (p>0.1, **Fig. 4d**). Therefore, the δ^{202}Hg values cannot be
299 used as a diagnostic tool for atmospheric transformation processes.

https://doi.org/10.5194/acp-2022-284
Preprint. Discussion started: 1 June 2022


Atmospheric Chemistry and Physics Discussions

However, the PBM samples with high Hg concentrations are characterized by negative δ^{202}Hg values, confirming the contribution from anthropogenic sources. These samples are related to the air mass from Bering Sea, coincide with enhanced levels of TGM observed in Bering Sea [45].

In addition to odd-MIF, the even-MIF is an important indicator for Hg sources and transformation processes in the atmosphere [16]. As shown in **Fig. 5**, the Δ^{200}Hg values were considered to be contributed by photochemical reactions in the upper troposphere. GEM oxidation could also induce even-MIF at low altitudes, but limited to specific oxidants (e.g., Br, Cl). This process could be identified by backward air mass trajectory as discussed below. The GEM oxidation processes without even-MIF, the resulting PBM generally inherited even-MIF signatures of GEM and RGM and was characterized by near-zero Δ^{200}Hg values. Here, we define PBM dominated by troposphere photochemical reactions are characterized by odd-MIF and significant even-MIF (Δ^{200}Hg≥0.15‰) and PBM dominated by GEM oxidation without even-MIF at low altitudes are characterized by negative odd-MIF and near-zero even-MIF at PBM. Therefore, except for samples with high Hg concentrations (anthropogenic emissions), most PBM samples were related with photoreduction (+odd-MIF), GEM oxidation (–odd-MIF), and troposphere photochemical reactions (+even-MIF), which could be identified by Δ^{199}Hg and Δ^{200}Hg values. Samples related with GEM oxidation are overlapped with PBM collected from polar

https://doi.org/10.5194/acp-2022-284
Preprint. Discussion started: 1 June 2022


Atmospheric Chemistry and Physics Discussions

region, which is also similar to GEM in terms of Δ^{199}Hg and Δ^{200}Hg values. According to previous study, these samples are primarily sourced from near-complete GEM oxidation [11,13]. As photoreduction induces no even-MIF and troposphere photochemical reactions are considered to induce even-MIF, samples with positive Δ^{199}Hg and near-zero Δ^{200}Hg values are believed to experience photoreduction rather than photo-oxidation and vice versa. Thus, the PBM samples could be classified into 6 types of different sources and atmospheric transformations based on Hg concentrations and isotope signatures (**Table 1**).

The ratio of Δ^{199}Hg to Δ^{201}Hg is commonly used to identify fractionation processes. The Δ^{199}Hg/Δ^{201}Hg ratio was 0.75 and 0.81 for the groups with positive and negative Δ^{199}Hg values, respectively (**Fig. S5a**). Both are lower than those observed for Hg(0) photo-oxidation (1.64–1.89) [42] and Hg(II) photo-reduction (1.00–1.31) [41,46], but higher than that in TGM from remote areas (0.73) [10,23,47] and coastal areas (0.55) [48,49]. The ratio lower than 1.00 has been presented in oxic experiments during photochemical reduction of Hg(II) [50]. These ratios indicated that the odd-MIF of PBM isotopes was induced by multiple processes rather than a single oxidation or reduction process. For each cruise, the ratio increased in the order Cruise A > Cruise B > Cruise C (**Fig. S5b**). With regards to the variations in latitude among the three cruises (**Table S2**), the ratios have a statistical correlation with mean latitude of each cruise (R^2=0.99, p<0.01).

https://doi.org/10.5194/acp-2022-284
Preprint. Discussion started: 1 June 2022


Atmospheric Chemistry and Physics Discussions

However, no correlations between the ratios and the corresponding mean Δ^{199}Hg value was found, which has been observed in PBM samples with highly positive Δ^{199}Hg from megacities [51]. Also, no correlations between odd-MIF and latitude for PBM were found (p>0.05). Similarly, no correlations between odd-MIF and radiation duration for PBM were observed (p>0.05, the radiation duration was represented by astronomical twilight which could be obtained from websites www.wunderground.com), which is inconsistent with a previous study [20] and implies potential impact of oxidations on the odd-MIF. It has been previously suggested that troposphere photochemical reactions that caused even-MIF was possibly accompanied by odd-MIF, although the magnitude is smaller than that induced by photoreduction [16]. Another reason maybe is that this study used ship-based sampling rather than fixed-point sampling, the baseline (background) PBM isotope signatures varied with sampling sites. Additionally, latitude was closely related with air temperature and light intensity, which may affect the MIF of PBM, but air temperature and light intensity were absent in this study. Nonetheless, the ratio for all PBM samples was 1.02 in this study, suggested odd-MIF was mainly caused by photochemical reactions and Δ^{199}Hg was a comprehensive result of different transformations.

The mechanism of even-MIF has been discussed for nearly a decade. Most scientists support the view that even-MIF is produced in the upper

https://doi.org/10.5194/acp-2022-284
Preprint. Discussion started: 1 June 2022


Atmospheric Chemistry and Physics Discussions

atmosphere and could be used to estimate the contribution of Hg from the upper troposphere [11,12,15,24]. Recent studies, however, propose a different mechanism in which small but significant Δ^{200}Hg anomalies can originate from *in situ* photooxidation of Hg(0) by UV light and oxidants at low altitudes [16,24,42]. Thus, we traced the air mass height of PBM samples during the past 13 days in comparison to the moment of sample collection (**Fig. S6**). This timeframe was selected because the global mean lifetime of Hg(II) before photoreduction in the troposphere is approximately 13 days [52]. The back trajectory model showed that air masses mainly (>90%) originated from below 1.5 km AMSL before arriving at the sampling sites in 21 out of 52 of the PBM samples, while air masses were completely derived from below 500 m AMSL in only 3 PBM samples (see **Methods; Table S4**). Highly positive Δ^{200}Hg values (≥0.15‰) were observed in 24 PBM samples. Discrete data points exhibited Δ^{200}Hg values that ranged from −0.11‰ to 0.14‰ (n=28). Here, we analyzed the relationships between Δ^{200}Hg values and frequencies of trajectory points when heights were higher than 500 m, 1500 m, and 3000 m AMSL (f_{500}, f_{1500}, and f_{3000}) (**Fig. 6a, b, and c**). Air masses mainly originated from low altitudes during Cruise A, because the mean frequencies were higher in Cruises B and C (48.08% for f_{500} and 27.17% for f_{1500}) than in Cruise A (25.33% for f_{500} and 11.41% for f_{1500}). Consequently, the latter mechanism in which even-MIF produced at low altitudes was dominant in shaping Δ^{200}Hg values of the

https://doi.org/10.5194/acp-2022-284
Preprint. Discussion started: 1 June 2022


Atmospheric Chemistry and Physics Discussions

PBM samples is supported by three lines of evidence: (1) highly positive Δ^{200}Hg values were positively correlated with multiple frequencies (i.e., f_{500}, f_{1500}, f_{3000}) during Cruise A, and the correlations were more significant at a lower altitude; (2) the positive relationships between highly positive Δ^{200}Hg values and frequencies f_{500} and f_{1500} were stronger in Cruise A than in Cruises B and C; and (3) significant negative relationships were observed between highly positive Δ^{200}Hg values and f_{3000} in Cruises B and C with more air masses from high altitudes. Moreover, the highly positive Δ^{200}Hg values in 6 PBM samples displayed f_{1500} = 0, indicating that these samples were associated with an air mass from low altitudes (<1.5 km) as the even-MIF in these samples was mainly produced at low altitudes. The mechanism could be due to vertical mixing of air masses from high and low altitudes, or photo-oxidation of Hg(0) at low altitudes. We also analyzed the frequencies as a function of height and light conditions; that is, when trajectory points occurred during day light (f_{500_light}, f_{1500_light}, and f_{3000_light}) (**Fig. 6d, e, and f**). The results showed that light played an important role in even-MIF, as Δ^{200}Hg and f_{500_light} (f_{1500_light}, f_{3000_light}) exhibited an analogous correlation to Δ^{200}Hg and f_{500} (f_{1500}, f_{3000}) (p>0.05, paired t test).

There would be a height that produce the max Δ^{200}Hg value in terms of the negative relationship between f_{3000} and Δ^{200}Hg, although the trend between f_{3000} and Δ^{200}Hg is completely opposite in Cruise A and in Cruise

https://doi.org/10.5194/acp-2022-284
Preprint. Discussion started: 1 June 2022


Atmospheric Chemistry and Physics Discussions

B and C, that is, the trend is opposite at low and high latitudes (**Fig. 6c**). In view of the fact that the tropospheric height decreases with the increase of latitude, the position of the same altitude relative to the tropopause (F_{position}) is different at high and low latitudes. For examples, we set the tropopause height at high and low latitudes to 9 km and 18 km, the position of 3000 m is 1/3 and 1/6 of the tropopause, respectively. Hence, we could obtain F_{position} = height/9000 at high latitudes and F_{position} = height/18000 at low latitudes, respectively. Fit F_{position} to the slope of Δ^{200}Hg and f_{500} (f_{1500}, f_{3000}) linearly (**Fig. S7**), the slope showed a negative linear correlation of the $F_{position}$, indicating that, as the height increases, the Δ^{200}Hg values first increases and then decreases. Hence, there should be a maximum Δ^{200}Hg values at a certain height. The fitting curve (r^2=0.95, p<0.01) intersects the x axis at 0.18, indicating that the max Δ^{200}Hg value would be produced at F_{position} = 0.18, that is, the max Δ^{200}Hg value would be produced at the height of 3240 m and 1620 m at low and high latitudes, respectively. Thus, the results confirmed the opposite trend between f_{3000} and Δ^{200}Hg at low and high latitudes. The max Δ^{200}Hg value was estimated by a Monte Carlo simulation approach and isotopic mixing model using data of type v which is dominated by troposphere photochemical reactions (see **Methods**). The estimated value of the max Δ^{200}Hg of 1.10±0.58 for PBM is overall similar to the maximum value (1.24 ± 0.08) currently observed in atmospheric environment [8].

https://doi.org/10.5194/acp-2022-284
Preprint. Discussion started: 1 June 2022


Atmospheric Chemistry and Physics Discussions

The precipitation samples are characterized by more positive Δ^{200}Hg values than PBM and GOM samples [16,17,27,53], suggesting that even-MIF produced in the MBL over the open ocean tend to be accumulated in aqueous phase and brought into seawater. The open ocean seawater shows positive Δ^{200}Hg values [54,55]. Latitudinal variations of Δ^{200}Hg were observed in seawater and precipitation, although negative correlation was found in seawater Δ^{200}Hg and latitudes and positive correlation was found in precipitation Δ^{200}Hg and latitudes, respectively [55,56]. As suggested, seawater Δ^{200}Hg are controlled by both Hg(0) and Hg(II) and larger ocean Hg(0) uptake at high latitudes results in low seawater Δ^{200}Hg [55]. While for precipitation Δ^{200}Hg, max Δ^{200}Hg values in the troposphere are estimated to be generated in lower altitudes at high latitudes, Δ^{200}Hg accumulated in precipitations would be less affected before reaching the ground (being collected).

As discussed above, photoreduction, troposphere photochemical reactions, and GEM oxidation are the three major processes that trigger odd-MIF and even-MIF (**Table 1**). Noted that adsorption and desorption between PBM and GOM induced no odd-MIF and the sources of Hg in the atmosphere are accompanied with near-zero odd-MIF [5,39,40]. Moreover, the Δ^{200}Hg values for GEM, GOM, and PBM are near-zero in source materials and therefore emissions [57]. Therefore, the Δ^{200}Hg and Δ^{199}Hg values could be used to estimate the contributions of photoreduction, photo-oxidation,

https://doi.org/10.5194/acp-2022-284
Preprint. Discussion started: 1 June 2022


Atmospheric Chemistry and Physics Discussions

and GEM oxidation. Here, we proposed two ways to quantify contributions from atmospheric transformations: (a) specific diagnostic ratios of $\Delta^{199}Hg/\Delta^{200}Hg$; (b) ternary isotopic mixing model.

(a) Even-odd patterns of Hg isotope fractionation factors have been proposed to be a better indicator of MIF mechanisms than $\Delta^{199}Hg/\Delta^{201}Hg$ slopes. According to previous study, a consistent pattern between $\Delta^{199}Hg$ and $\Delta^{200}Hg$ has been observed with large variation range (1.1-3.3) on GEM and oxidized Hg phases (i.e., reactive Hg and precipitation Hg) [16,48,58]. As listed in Table 1, samples in type i could be used to represent near-complete GEM oxidation and inherit the isotope composition of GEM. We then built $\Delta^{199}Hg/\Delta^{200}Hg$ slopes between type i and type ii, iii, and v, respectively. Based on Williamson-York bivariate linear regression method [59], the observed fitted curve shaped a slope of 1.81±0.27 (r^2=0.57, p<0.01), 4.90±0.82 (r^2=0.31, p<0.05), and 0.03±0.16 (r^2=0.00, p=0.94), respectively. We suggest that the slope was primarily determined by the isotope signatures of oxidized Hg phases, because GEM varies in a narrow range of $\Delta^{199}Hg$ and $\Delta^{200}Hg$ with -0.20±0.17‰ and -0.06±0.12‰ (2SD, n=208), respectively [9,10,13,16,44,48,58,60-63]. Thus, we hypothesized that the ratios of $\Delta^{199}Hg/\Delta^{200}Hg$ could be used as a diagnostic for proportions of photoreduction and troposphere photochemical reactions despite of GEM oxidation. To gain a more representative result, we integrate our data with a subset of the published PBM data (**Fig. 7**). The resulting ratios of

https://doi.org/10.5194/acp-2022-284
Preprint. Discussion started: 1 June 2022


Atmospheric Chemistry and Physics Discussions

476 $\Delta^{199}Hg/\Delta^{200}Hg$ were 17.71±1.42 (r^2=0.27, p<0.01) and 0.61±0.06 (r^2=0.43,
477 p<0.01) for photoreduction-dominated and troposphere-oxidation-
478 dominated PBM samples, respectively. The proportions of photoreduction
479 and photo-oxidation could be calculated as the equation below:

480 $$f_{red} = \frac{\arctan(k) - arctan0.61}{arctan17.71 - arctan0.61} \times 100\% = \frac{arctan(k) - 0.548}{0.966} \times 100\% \quad (1)$$

481 where f_{red} represents proportions of photoreduction and k represent ratios
482 of $\Delta^{199}Hg/\Delta^{200}Hg$. Following equation (1), we suggested that 66±16% of
483 Hg was photoreduced in precipitation and 75±16% Hg was photoreduced
484 in oxidized Hg phases at high altitudes (**Table S6**). In this study, the f_{red}
485 was calculated for sample types ii, iii, and v and listed in **Table 1**. It should
486 be noted again that the f_{red} was calculated without considering the influence
487 of GEM oxidation. If GEM oxidation effects greatly, such as the observed
488 $\Delta^{199}Hg$ values are near-zero or negative, the ratios would be useless. For
489 example, the calculated f_{red} for sample types v was -0.58 and meaningless.

490 (b) As shown in **Fig. 7**, the three end-member could be used to
491 calculate contributions from photoreduction, troposphere photochemical
492 reactions, and GEM oxidation through ternary isotopic mixing model.

493 $$X \cdot \Delta^{200}Hg_{red} + Y \cdot \Delta^{200}Hg_{oxi} + Z \cdot \Delta^{200}Hg_{GEMo} = \Delta^{200}Hg_{sam} \quad (2)$$

494 $$X \cdot \Delta^{199}Hg_{red} + Y \cdot \Delta^{199}Hg_{oxi} + Z \cdot \Delta^{199}Hg_{GEMo} = \Delta^{199}Hg_{sam} \quad (3)$$

495 $$X + Y + Z = 1 \quad (4)$$

496 where X, Y, and Z represent the contribution of the three atmospheric
497 transformations of the photoreduction, troposphere photochemical

https://doi.org/10.5194/acp-2022-284
Preprint. Discussion started: 1 June 2022


Atmospheric Chemistry and Physics Discussions

reactions, and GEM oxidation, respectively. The Hg isotope signatures of the three atmospheric transformations are the mean values of the three end-member as mentioned above (**Table S5**). The results of the mixing model calculation showed that the contributions of photoreduction, troposphere photochemical reactions, and GEM oxidation varied within -12% to 77%, -12% to 35%, and 2% to 97%, respectively (**Table 1**). The results showed similar contribution from photoreduction with estimations from ratios of $\Delta^{199}Hg/\Delta^{200}Hg$. The estimated highly contributions (53±22%, 1SD) of GEM oxidation is consistent with previous suggestion that GEM oxidation played a major role (~47±22%) in the formation of Hg(II) in PBM [17,51]. The weak contributions (10±12%, 1SD) of troposphere photochemical reactions indicate strong dilutions of near-zero $\Delta^{200}Hg$ from Hg sources and other atmospheric transformations.

5. Conclusion

The isotopic compositions of PBM in the MBL of the Northwest Pacific suggest that the even-MIF and odd-MIF signatures are useful tracers for identifying atmospheric transformations. The $\delta^{202}Hg$ signature was significantly shifted by Hg sources and *in situ* transformations of atmospheric Hg. Strong correlations between the even-MIF of PBM and height of the air mass provide additional support for the occurrence of even-MIF in the troposphere, which may link to photochemical reactions

https://doi.org/10.5194/acp-2022-284
Preprint. Discussion started: 1 June 2022


Atmospheric Chemistry and Physics Discussions

in the atmosphere. The mechanism driving the highly positive Δ^{200}Hg signatures of PBM in this study is probably the oxidation of Hg(0) at low altitudes. The MBL over the open ocean may promote the intrusion of even-MIF signatures and its subsequent recording by seawater and marine sediments [55,64,65]. It is highly uncertain how strong even-MIF signatures could be generated in the troposphere, the estimated max Δ^{200}Hg value provides data support for future research. The quantification of contributions of atmospheric transformations by the proposed methods have implications for the study of Hg behaviors in the atmosphere.

Description of statistical analysis. All the statistical analyses were performed using Origin 2019b and Excel 2019. The Paired *t*-test, Pearson's R-Square and *P*-value are calculated by algorithms of the software.

Data availability. The authors declare that the main data supporting the findings of this study are available within the paper and its supplementary information files. Extra data are available from the corresponding author upon request.

Author contributions

S.H., and Y.Z.* conceived and designed this project, S.H., Y.H., and H.S. conducted the field sampling, S.H., S.L., Y.Z., and Y.C. carried out all the

https://doi.org/10.5194/acp-2022-284
Preprint. Discussion started: 1 June 2022


Atmospheric Chemistry and Physics Discussions

542 measurements, and S.H., K.L., and Y.Z.* wrote the draft paper.

543

544 **Competing interests**

545 The authors declare no competing interests.

546

547 **Additional information**

548 Correspondence and requests for materials should be addressed to Y.Z.

549

550 **Acknowledgments**

551 This research was financed by the National Science Foundation for
552 Young Scientists of China (22006168), the National Key Research and
553 Development Program of China (2019YFA0607003), the Chinese Projects
554 for Investigations and Assessments of the Arctic and Antarctic
555 (CHINARE2017-2021), and the Natural Science Foundation of Fujian
556 Province, China (2020J05074). The authors acknowledge the support of
557 the Fujian Science and Technology Innovation Leader Project 2016. We
558 thank LetPub (www.letpub.com) for linguistic assistance and pre-
559 submission expert review.

560

561 **References:**

562 1 Schroeder, W. & Munthes, J. Atmospheric Mercury - An Overview. *Atmos. Environ.* **32**,
563 809-822 (1998).
564 2 Mao, H., Cheng, I. & Zhang, L. Current understanding of the driving mechanisms for
565 spatiotemporal variations of atmospheric speciated mercury: a review. *Atmos. Chem. Phys.*

https://doi.org/10.5194/acp-2022-284
Preprint. Discussion started: 1 June 2022

16, 12897-12924, doi:10.5194/acp-16-12897-2016 (2016).

3 Gustin, M. S., Amos, H. M., Huang, J., Miller, M. B. & Heidecorn, K. Measuring and modeling mercury in the atmosphere: a critical review. *Atmos. Chem. Phys.* **15**, 5697-5713, doi:10.5194/acp-15-5697-2015 (2015).

4 Sun, R. *et al.* Modelling the mercury stable isotope distribution of Earth surface reservoirs: Implications for global Hg cycling. *Geochim. Cosmochim. Acta* **246**, 156-173 (2018).

5 Das, R. *et al.* Mercury isotopes of atmospheric particle bound mercury for source apportionment study in urban Kolkata, India. *Elementa-Sci. Anthrop.* **4**, 12 (2016).

6 Douglas, T. & Blum, J. Mercury Isotopes Reveal Atmospheric Gaseous Mercury Deposition Directly to the Arctic Coastal Snowpack. *Environ. Sci. Technol. Let.* **6**, 235-242 (2019).

7 Blum, J., Sherman, L. & Johnson, M. Mercury Isotopes in Earth and Environmental Sciences. *Annu. Rev. Earth Planet. Sci.* **42**, 249-269 (2014).

8 Chen, J., Hintelmann, H., Feng, X. & Dimock, B. Unusual fractionation of both odd and even mercury isotopes in precipitation from Peterborough, ON, Canada. *Geochim. Cosmochim. Acta* **90**, 33-46 (2012).

9 Rolison, J., Landing, W., Luke, W., Cohen, M. & Salters, V. Isotopic composition of species-specific atmospheric Hg in a coastal environment. *Chem. Geol.* **336**, 13 (2013).

10 Demers, J., Blum, J. & Zak, D. Mercury isotopes in a forested ecosystem: Implications for air-surface exchange dynamics and the global mercury cycle. *Global Biogeochem. Cycles* **27**, 222-238 (2013).

11 Li, C. *et al.* Seasonal Variation of Mercury and Its Isotopes in Atmospheric Particles at the Coastal Zhongshan Station, Eastern Antarctica. *Environ Sci Technol* **54**, 11344-11355, doi:10.1021/acs.est.0c04462 (2020).

12 Jiskra, M., Sonke, J., Agnan, Y., Helmig, D. & Obrist, D. Insights from mercury stable isotopes on terrestrial–atmosphere exchange of Hg(0) in the Arctic tundra. *Biogeosciences* **16**, 4051-4064 (2019).

13 Zheng, W. *et al.* Mercury stable isotopes reveal the sources and transformations of atmospheric Hg in the high Arctic. *Appl. Geochem.* **131**, 105002, doi:10.1016/j.apgeochem.2021.105002 (2021).

14 Huang, S., Lin, K., Yuan, D., Gao, Y. & Sun, L. Mercury isotope fractionation during transfer from post-desulfurized seawater to air. *Mar. Pollut. Bull.* **113**, 81-86 (2016).

15 Cai, H. & Chen, J. Mass-independent fractionation of even mercury isotopes. *Sci. Bull.* **61**, 116-124 (2016).

16 Fu, X. *et al.* Mass-Independent Fractionation of Even and Odd Mercury Isotopes during Atmospheric Mercury Redox Reactions. *Environ Sci Technol* **55**, 10164-10174, doi:10.1021/acs.est.1c02568 (2021).

17 Yu, B. *et al.* New evidence for atmospheric mercury transformations in the marine boundary layer from stable mercury isotopes. *Atmos. Chem. Phys.* **20**, 9713-9723, doi:10.5194/acp-20-9713-2020 (2020).

18 Meng, M. *et al.* Mercury Inputs Into Eastern China Seas Revealed by Mercury Isotope Variations in Sediment Cores. *Journal of Geophysical Research: Oceans* **126**, doi:10.1029/2020jc016891 (2021).

19 Qiu, Y. *et al.* Identification of potential sources of elevated PM2.5-Hg using mercury isotopes during haze events. *Atmos. Environ.* **247**, 118203,

https://doi.org/10.5194/acp-2022-284
Preprint. Discussion started: 1 June 2022

doi:10.1016/j.atmosenv.2021.118203 (2021).

20 Huang, Q. *et al.* Diel variation of mercury stable isotope ratios record photoreduction of PM2.5-bound mercury. *Atmos. Chem. Phys.*, 315-325 (2019).

21 Huang, S. *et al.* Natural stable isotopic compositions of mercury in aerosols and wet precipitations around a coal-fired power plant in Xiamen, southeast China. *Atmos. Environ.* **173**, 72-80 (2018).

22 Xu, H. *et al.* Mercury stable isotope compositions of Chinese urban fine particulates in winter haze days: Implications for Hg sources and transformations. *Chem. Geol.* **504**, 267-275 (2018).

23 Yu, B. *et al.* Isotopic Composition of Atmospheric Mercury in China: New Evidence for Sources and Transformation Processes in Air and in Vegetation. *Environ. Sci. Technol.* **50**, 9262-9269 (2016).

24 Fu, X. *et al.* Domestic and Transboundary Sources of Atmospheric Particulate Bound Mercury in Remote Areas of China: Evidence from Mercury Isotopes. *Environ. Sci. Technol.* **53**, 1947-1957 (2019).

25 Hedgecock, I. & Pirrone, N. Chasing quicksilver: Modeling the atmospheric lifetime of Hg0 (g) in the marine boundary layer at various latitudes. *Environ. Sci. Technol.* **38**, 69–76 (2004).

26 Hedgecock, I. & Pirrone, N. Mercury and photochemistry in the marine boundary layer-modelling studies suggest the in situ production of reactive gas phase mercury. *Atmos. Environ.* **35**, 3055–3062 (2001).

27 Qiu, Y. *et al.* Stable mercury isotopes revealing photochemical processes in the marine boundary layer. *J. Geophys. Res.: Atmos.*, doi:10.1029/2021jd034630 (2021).

28 Stein, A. F. *et al.* NOAA's HYSPLIT Atmospheric Transport and Dispersion Modeling System. *Bull. Am. Meteorol. Soc.* **96**, 2059-2077, doi:10.1175/bams-d-14-00110.1 (2015).

29 Rolph, G., Stein, A. & Stunder, B. Real-time Environmental Applications and Display sYstem: READY. *Environ. Modell. Softw.* **95**, 210-228, doi:10.1016/j.envsoft.2017.06.025 (2017).

30 Huang, Q. *et al.* An improved dual-stage protocol to preconcentrate mercury from airborne particles for precise isotopic measurement. *J. Anal. At. Spectrom.* **30**, 966 (2015).

31 Huang, S. *et al.* Application of an isotope binary mixing model for determination of precise mercury isotopic composition in samples with low mercury concentration. *Anal. Chem.* **91**, 7063-7069 (2019).

32 Lin, H. *et al.* Isotopic composition analysis of dissolved mercury in seawater with purge and trap preconcentration and a modified Hg introduction device for MC-ICPMS. *J. Anal. At. Spectrom.* **30**, 353-359 (2015).

33 Blum, J. & Bergquist, B. Reporting of variations in the natural isotopic composition of mercury. *Anal. Bioanal. Chem.* **388**, 359 (2007).

34 Janssen, S. E. *et al.* Examining historical mercury sources in the Saint Louis River estuary: How legacy contamination influences biological mercury levels in Great Lakes coastal regions. *Sci. Total Environ.* **779**, 146284, doi:10.1016/j.scitotenv.2021.146284 (2021).

35 Enrico, M., Balcom, P., Johnston, D. T., Foriel, J. & Sunderland, E. M. Simultaneous combustion preparation for mercury isotope analysis and detection of total mercury using a direct mercury analyzer. *Anal. Chim. Acta* **1154**, 338327, doi:10.1016/j.aca.2021.338327

https://doi.org/10.5194/acp-2022-284
Preprint. Discussion started: 1 June 2022

(2021).

36 Timonen, H., Ambrose, J. L. & Jaffe, D. A. Oxidation of elemental Hg in anthropogenic and marine airmasses. *Atmos. Chem. Phys.* **13**, 2827-2836, doi:10.5194/acp-13-2827-2013 (2013).

37 Huang, Q., Reinfelder, J., Fu, P. & Huang, W. Variation in the mercury concentration and stable isotope composition of atmospheric total suspended particles in Beijing, China. *J. Hazard. Mater.* **383**, 121131 (2019).

38 Huang, Q. *et al.* Isotopic composition for source identification of mercury in atmospheric fine particles. *Atmos. Chem. Phys.* **16**, 14 (2016).

39 Li, X. *et al.* Isotope signatures of atmospheric mercury emitted from residential coal combustion. *Atmos. Environ.* **246**, 118175, doi:10.1016/j.atmosenv.2020.118175 (2021).

40 Zambardi, T., Sonke, J., Toutain, J., Sortino, F. & Shinohara, H. Mercury emissions and stable isotopic compositions at Vulcano Island (Italy). *Earth and Planetary Science Letters* **277**, 236-243 (2009).

41 Bergquist, B. & Blum, J. Mass-Dependent and -Independent Fractionation of Hg Isotopes by Photoreduction in Aquatic Systems. *Science* **318**, 417-420 (2007).

42 Sun, G. *et al.* Mass-Dependent and -Independent Fractionation of Mercury Isotope during Gas-Phase Oxidation of Elemental Mercury Vapor by Atomic Cl and Br. *Environ. Sci. Technol.* **50**, 9232-9241 (2016).

43 Fu, X. *et al.* Isotopic compositions of atmospheric total gaseous mercury in ten Chinese cities and implications for land surface emissions. *Atmos. Chem. Phys.*, Preprint, doi:10.5194/acp-2020-981 (2021).

44 Fu, X., Marusczak, N., Wang, X., Gheusi, F. & Sonke, J. Isotopic Composition of Gaseous Elemental Mercury in the Free Troposphere of the Pic du Midi Observatory, France. *Environ. Sci. Technol.* **50**, 5641-5650 (2016).

45 Kang, H. & Xie, Z. Atmospheric mercury over the marine boundary layer observed during the third China Arctic Research Expedition. *Journal of Environmental Sciences* **23**, 1424-1430, doi:10.1016/s1001-0742(10)60602-x (2011).

46 Zheng, W. & Hintelmann, H. Mercury isotope fractionation during photoreduction in natural water is controlled by its Hg/DOC ratio. *Geochim. Cosmochim. Acta* **73**, 6704-6715 (2009).

47 Fu, X. *et al.* Significant Seasonal Variations in Isotopic Composition of Atmospheric Total Gaseous Mercury at Forest Sites in China Caused by Vegetation and Mercury Sources. *Environ. Sci. Technol.* (2019).

48 Demers, J., Sherman, L., Blum, J., Marsik, F. & Dvonch, J. Coupling atmospheric mercury isotope ratios and meteorology to identify sources of mercury impacting a coastal urban-industrial region near Pensacola, Florida, USA. *Global Biogeochem. Cycles* **29**, 17 (2015).

49 Fu, X. *et al.* Isotopic Composition of Gaseous Elemental Mercury in the Marine Boundary Layer of East China Sea. *J. Geophys. Res. - Atmos.* (2018).

50 Motta, L. C., Kritee, K., Blum, J. D., Tsz-Ki Tsui, M. & Reinfelder, J. R. Mercury Isotope Fractionation during the Photochemical Reduction of Hg(II) Coordinated with Organic Ligands. *J. Phys. Chem. A* **124**, 2842-2853, doi:10.1021/acs.jpca.9b06308 (2020).

51 Liu, C. *et al.* Sources and Transformation Mechanisms of Atmospheric Particulate Bound Mercury Revealed by Mercury Stable Isotopes. *Environ Sci Technol*,

https://doi.org/10.5194/acp-2022-284
Preprint. Discussion started: 1 June 2022

698 doi:10.1021/acs.est.1c08065 (2022).
699 52 Horowitz, H. M. *et al.* A new mechanism for atmospheric mercury redox chemistry:
700 Implications for the global mercury budget. *Atmos. Chem. Phys.* **17**, 6353-6371,
701 doi:10.5194/acp-2016-1165 (2017).
702 53 Motta, L. *et al.* Mercury Cycling in the North Pacific Subtropical Gyre as Revealed by
703 Mercury Stable Isotope Ratios. *Global Biogeochem. Cycles* **33**, 777-794 (2019).
704 54 Štrok, M., Baya, P. & Hintelmann, H. The mercury isotope composition of Arctic coastal
705 seawater. *C.R. Geosci.* **347**, 368-376 (2015).
706 55 Jiskra, M. *et al.* Mercury stable isotopes constrain atmospheric sources to the Ocean.
707 *Nature* **597**, 678-682 (2021).
708 56 Wang, Z. *et al.* Mass-dependent and mass-independent fractionation of mercury isotopes
709 in precipitation from Guiyang, SW China. *C.R. Geosci.* **347**, 358-367 (2015).
710 57 Sun, R. *et al.* Historical (1850–2010) mercury stable isotope inventory from anthropogenic
711 sources to the atmosphere. *Elementa-Sci. Anthrop.* **4**, 000091 (2016).
712 58 Gratz, L., Keeler, G., Blum, J. & Sherman, L. Isotopic Composition and Fractionation of
713 Mercury in Great Lakes Precipitation and Ambient Air. *Environ. Sci. Technol.* **44**, 7770
714 (2010).
715 59 Cantrell, C. A. Technical Note: Review of methods for linear least-squares fitting of data
716 and application to atmospheric chemistry problems. *Atmos. Chem. Phys.* **8**, 5477-5487
717 (2008).
718 60 A. Yamakawa, A. T., Y. Takeda, S. Kato and Y. Kajii. Emerging investigator series:
719 investigation of mercury emission sources using Hg isotopic compositions of atmospheric
720 mercury at the Cape Hedo Atmosphere and Aerosol Monitoring Station (CHAAMS), Japan.
721 *Environmental Science Processes & Impacts* (2019).
722 61 Akane Yamakawa, K. M., Jun Yoshinaga. Determination of isotopic composition of
723 atmospheric mercury in urban-industrial and coastal regions of Chiba, Japan, using cold
724 vapor multicollector inductively coupled plasma mass spectrometry. *Chem. Geol.* **448**, 9
725 (2017).
726 62 Kurz, A. Y., Blum, J. D., Johnson, M. W., Nadelhoffer, K. & Zak, D. R. Isotopic composition
727 of mercury deposited via snow into mid-latitude ecosystems. *Sci. Total Environ.* **784**,
728 147252, doi:10.1016/j.scitotenv.2021.147252 (2021).
729 63 Yu, B. *et al.* Katabatic Wind and Sea-Ice Dynamics Drive Isotopic Variations of Total
730 Gaseous Mercury on the Antarctic Coast. *Environ Sci Technol* **55**, 6449-6458,
731 doi:10.1021/acs.est.0c07474 (2021).
732 64 Yin, R. *et al.* Mercury Inputs to Chinese Marginal Seas – Impact of Industrialization and
733 Development of China. *Journal of Geophysical Research: Oceans* **123**, 5599-5611 (2018).
734 65 Zerkle, A. L. *et al.* Anomalous fractionation of mercury isotopes in the Late Archean
735 atmosphere. *Nat Commun* **11**, 1709, doi:10.1038/s41467-020-15495-3 (2020).
736 66 Guo, J. *et al.* Source identification of atmospheric particle-bound mercury in the
737 Himalayan foothills through non-isotopic and isotope analyses. *Environ. Pollut.* **286**,
738 117317, doi:10.1016/j.envpol.2021.117317 (2021).

739

740

https://doi.org/10.5194/acp-2022-284
Preprint. Discussion started: 1 June 2022

Atmospheric Chemistry and Physics Discussions

741

https://doi.org/10.5194/acp-2022-284
Preprint. Discussion started: 1 June 2022

Atmospheric Chemistry and Physics Discussions

742 Table 1 The possible Hg sources and atmospheric transformations for PBM

743 samples and the estimated contributions

ID	X	Y	Z	f_{red}^{*} (%)	f_{red}^{**} (%)
Type i. GEM oxidation (negative Δ^{199}Hg and near-zero Δ^{200}Hg)					
16	0.13	-0.02	0.89	N.A.	N.A.
25	0.14	-0.01	0.87		
26	0.14	-0.09	0.95		
37	0.15	-0.09	0.94		
Type ii. Photoreduction & troposphere photochemical reactions (positive Δ^{199}Hg and Δ^{200}Hg)					
5	0.50	0.17	0.33		
6	0.46	0.18	0.36		
7	0.34	0.33	0.33		
14	0.58	0.12	0.30		
19	0.65	0.10	0.25		
20	0.57	0.19	0.24		
23	0.77	0.21	0.02		
28	0.26	0.19	0.55	54±29	70±11
32	0.61	0.27	0.13		
34	0.31	0.31	0.38		
35	0.37	0.25	0.38		
36	0.52	0.17	0.31		
39	0.42	0.10	0.47		
42	0.36	0.24	0.40		
43	0.50	0.16	0.34		
Type iii. Photoreduction (positive Δ^{199}Hg and near-zero Δ^{200}Hg)					
4	0.64	-0.03	0.39		
8	0.54	-0.02	0.48		
9	0.45	-0.08	0.63		
10	0.48	0.08	0.44		
13	0.54	-0.06	0.53		
15	0.34	0.10	0.55		
21	0.38	0.09	0.53		
22	0.55	0.04	0.41		
24	0.74	-0.10	0.35	85±14	100±14
27	0.50	-0.12	0.61		
30	0.45	0.09	0.46		
31	0.59	0.04	0.37		
41	0.57	0.03	0.40		
44	0.62	0.02	0.37		
45	0.74	-0.03	0.29		
50	0.53	-0.01	0.48		
51	0.58	0.00	0.42		

https://doi.org/10.5194/acp-2022-284
Preprint. Discussion started: 1 June 2022

Atmospheric Chemistry and Physics Discussions

Type iv. GEM oxidation & photoreduction (slightly negative Δ^{199}Hg and near-zero Δ^{200}Hg)					
2	0.31	0.04	0.65	N.A.	N.A.
11	0.28	0.09	0.63		
33	0.31	-0.01	0.71		
38	0.25	0.08	0.67		
Type v. troposphere photochemical reactions (negative Δ^{199}Hg and positive Δ^{200}Hg)					
1	-0.12	0.34	0.78		
3	0.11	0.19	0.69		
12	-0.07	0.35	0.72		
17	0.12	0.24	0.64		
18	-0.10	0.13	0.97	-58±41	-37±128
29	0.00	0.27	0.73		
40	-0.06	0.23	0.83		
46	0.15	0.15	0.70		
52	0.07	0.21	0.72		
Type vi. Anthropogenic emissions (slightly negative Δ^{199}Hg and high Hg concentrations)					
47	0.29	-0.03	0.73		
48	0.26	0.04	0.70	N.A.	N.A.
49	0.23	0.06	0.70		
mean	0.37	0.10	0.53		
sd	0.23	0.12	0.22		

744 *The f_{red} was calculated from ratios of Δ^{199}Hg/Δ^{200}Hg.

745 ** The f_{red} was calculated from X/(X+Y)

746

https://doi.org/10.5194/acp-2022-284
Preprint. Discussion started: 1 June 2022

Atmospheric Chemistry and Physics Discussions

747 **Figures**

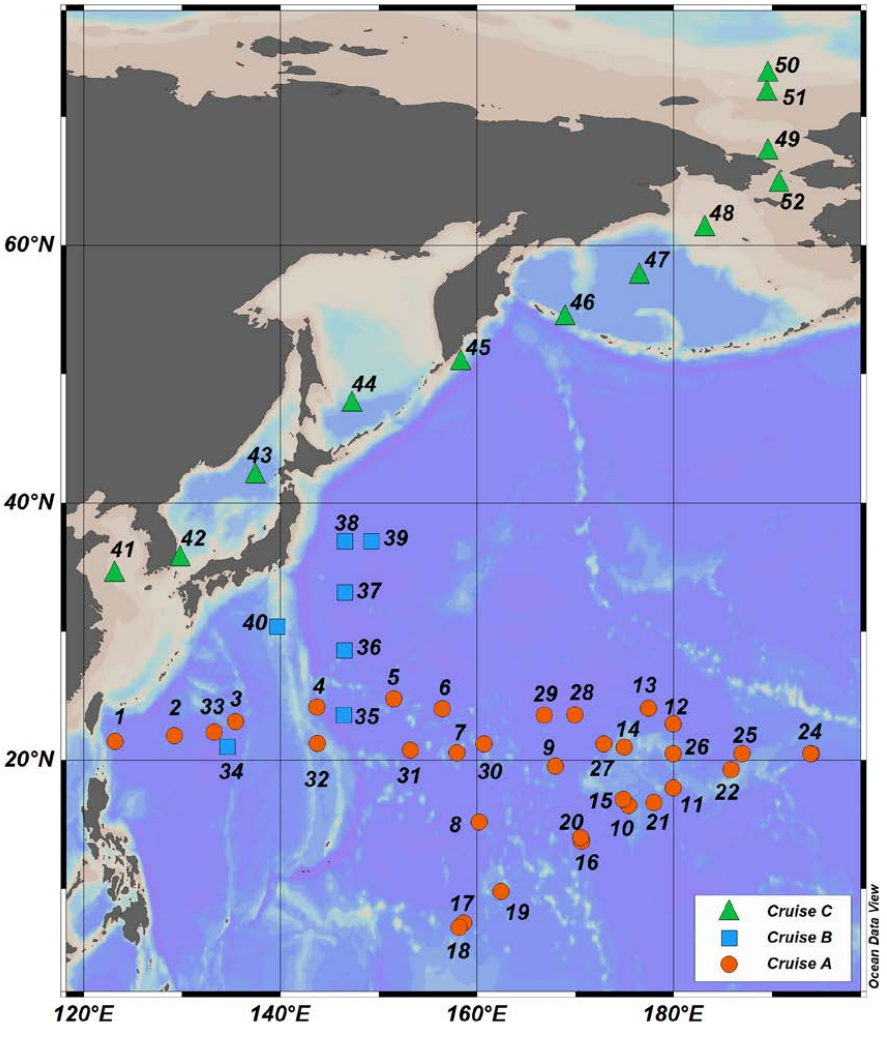

748 Figure 1. Map of sampling locations. The points represent the locations
749 at the "midpoint" moment during the sampling time of PBM samples.
750 (Ocean Data View 2020)

751

https://doi.org/10.5194/acp-2022-284
Preprint. Discussion started: 1 June 2022

Atmospheric Chemistry and Physics Discussions

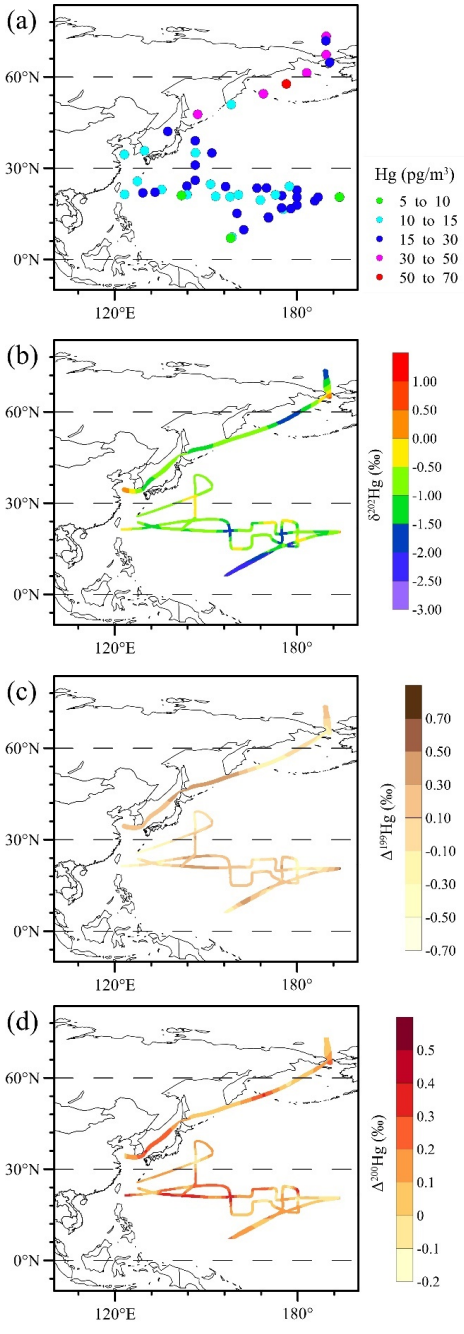

752 Figure 2. Spatial distributions of (a) Hg concentrations, (b) δ^{202}Hg, (c)

753 Δ^{199}Hg, and (d) Δ^{200}Hg of PBM in the MBL of the Northwest Pacific.

https://doi.org/10.5194/acp-2022-284
Preprint. Discussion started: 1 June 2022

Atmospheric Chemistry and Physics Discussions

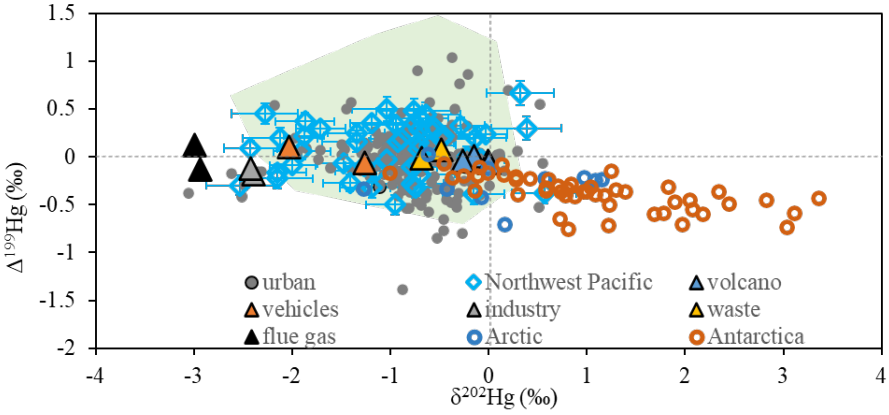

754 Figure 3. Plot of Δ^{199}Hg vs. δ^{202}Hg for PBM in the Northwest Pacific from
755 this study, along with isotope data for PBM reported in the literature. The
756 references for the literature data are: urban [19-23,37,38], volcano [40],
757 traffic/vehicles [5], industry [5], waste [5], flue gas [39], arctic [13], antarctica [11], and
758 high altitude areas (the green zone)[23,24].

759

https://doi.org/10.5194/acp-2022-284
Preprint. Discussion started: 1 June 2022

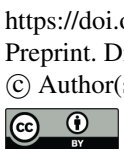

Atmospheric Chemistry and Physics Discussions

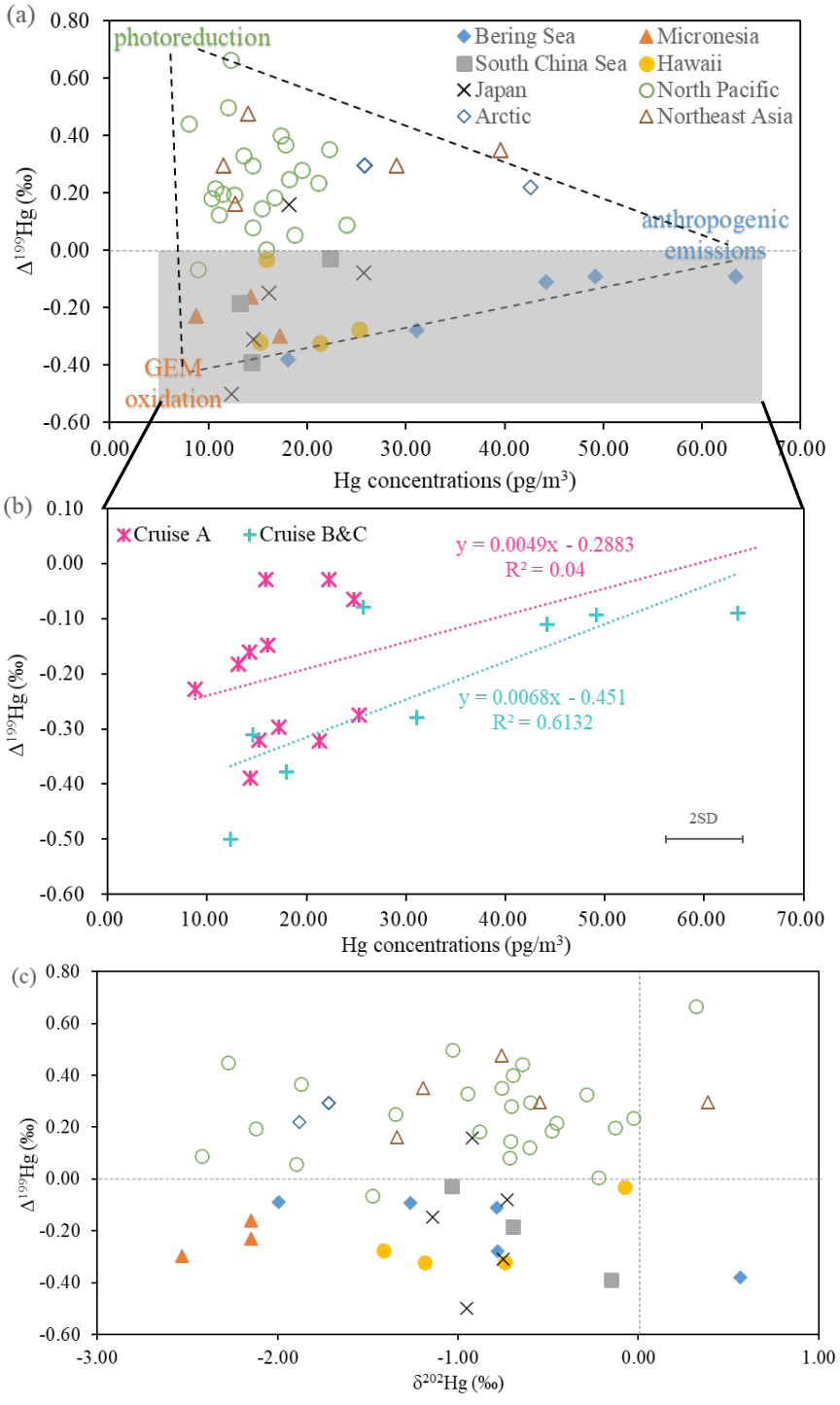

https://doi.org/10.5194/acp-2022-284
Preprint. Discussion started: 1 June 2022

Atmospheric Chemistry and Physics Discussions

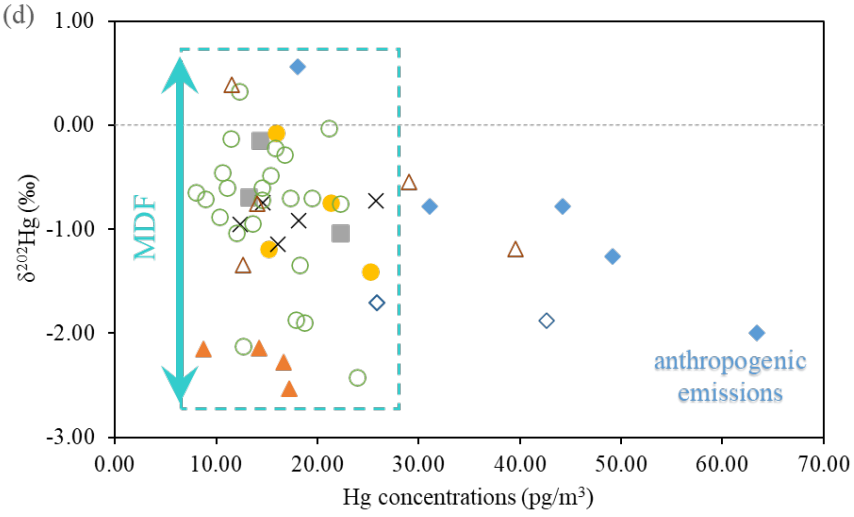

761 Figure 4. (a) Plot of Δ^{199}Hg vs. Hg concentration for PBM samples. (b)
762 Plot of Δ^{199}Hg vs. Hg concentration for negative Δ^{199}Hg values of PBM
763 during the different cruises. (c) Plot of Δ^{199}Hg vs. δ^{202}Hg for PBM samples.
764 (d) Plot of δ^{202}Hg vs. Hg concentration for PBM samples. The error bar
765 represents ±2SD for Hg concentrations. The typical 2SD analytic
766 uncertainty of PBM samples was 0.22‰ to 0.42‰ and 0.07‰ to 0.13‰
767 for δ^{202}Hg and Δ^{199}Hg, respectively, and listed in **Table S2**.
768

https://doi.org/10.5194/acp-2022-284
Preprint. Discussion started: 1 June 2022

Atmospheric Chemistry and Physics Discussions

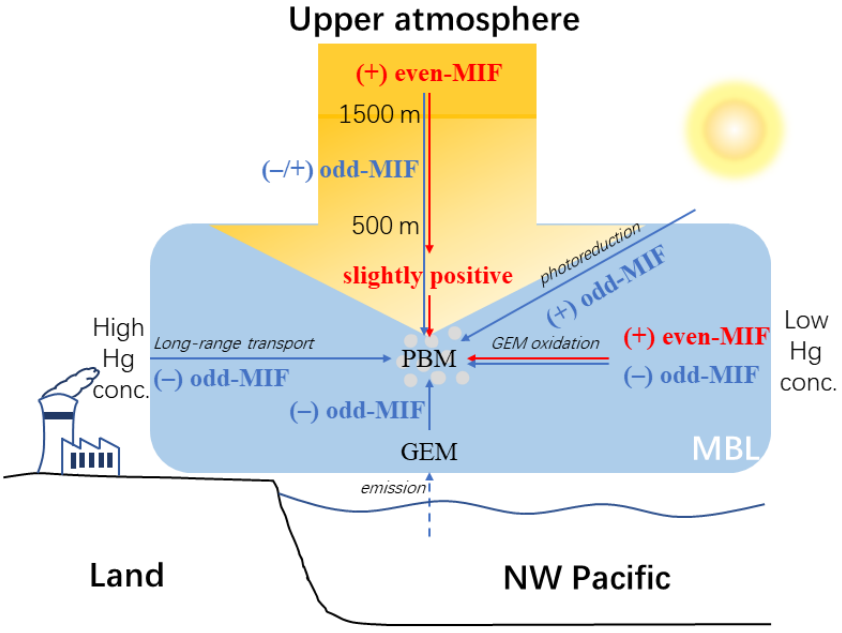

769 Figure 5. Schematic diagram of possible Hg sources and transformation

770 processes for PBM over the MBL.

771

https://doi.org/10.5194/acp-2022-284
Preprint. Discussion started: 1 June 2022

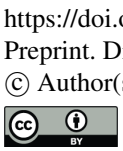

Atmospheric Chemistry and Physics Discussions

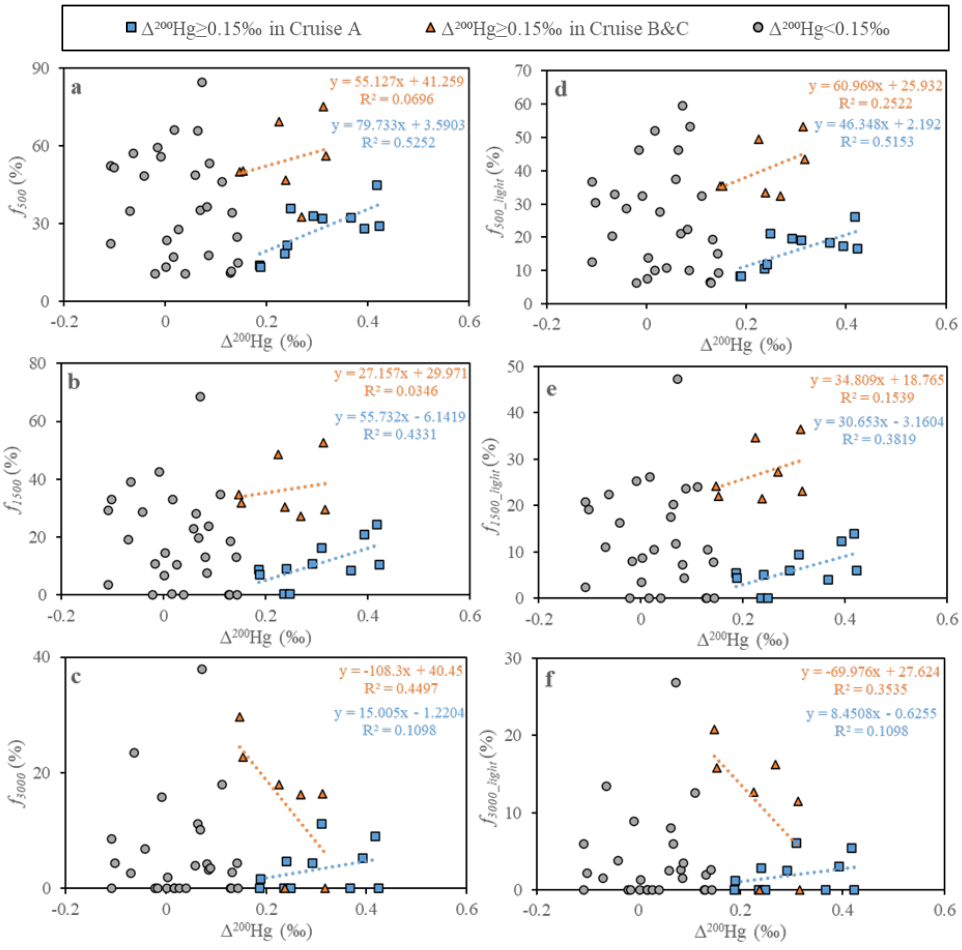

772 Figure 6. Plots of (a) f_{500}, (b) f_{1500}, (c) f_{3000}, (d) f_{500_light}, (e) f_{1500_light}, and (f)
773 f_{3000_light} vs. Δ^{200}Hg. The square and triangle represent PBM samples during
774 Cruise A and Cruises B&C, respectively. The circles represent PBM
775 samples with Δ^{200}Hg values lower than 0.15‰.

776

https://doi.org/10.5194/acp-2022-284
Preprint. Discussion started: 1 June 2022

Atmospheric Chemistry and Physics Discussions

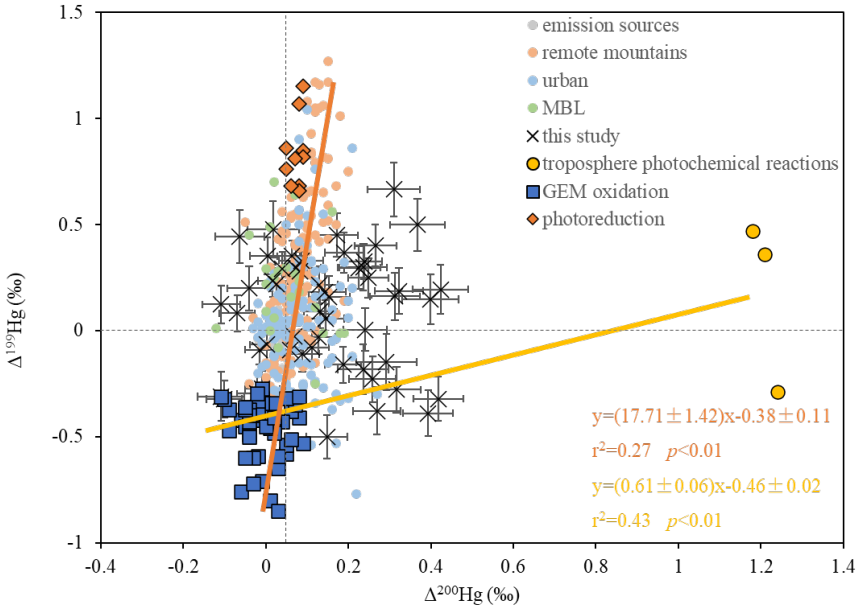

Figure 7. Plot of Δ^{199}Hg vs. Δ^{200}Hg for PBM samples collected from emission sources [5,39,40], remote mountains [23,24,66], urban [19-23,38], MBL [17,27], and this study. The three end-members of troposphere photochemical reactions, GEM oxidation, and photoreduction are compiled from the literature (**Table S5**). The criteria for the selection of the published Hg isotope data are following: samples (mainly in remoted mountains) with highly positive Δ^{199}Hg (>0.66‰) and near-zero Δ^{200}Hg values are supposed to be dominated by photoreduction [24]; samples (mainly in precipitation) with highly positive Δ^{200}Hg (>1.10‰) values are supposed to be dominated by troposphere photochemical reactions [8]; samples (mainly in polar regions) with negative Δ^{199}Hg (<-0.30‰) and near-zero Δ^{200}Hg values are supposed to be dominated by GEM oxidation [11,13,20,21,27].

https://doi.org/10.5194/acp-2022-284
Preprint. Discussion started: 1 June 2022

Atmospheric Chemistry and Physics Discussions

789 Error bars represent the 2SD uncertainties of individual samples.